ACS MATERIALS LETTERS

www.acsmaterialsletters.org

Improved Thermal Stability and Operational Lifetime of Blue Fluorescent Organic Light-Emitting Diodes by Using a Mixed-Electron Transporting Layer

Min Seok Ki,[▽] Myungsun Sim,[▽] Ohyun Kwon,*[,▽] Kyuhyun Im, Byoungki Choi,* Byeong Jun Cha, Young Dok Kim, Tae Young Jin, and Keewook Paeng*

Cite This: *ACS Materials Lett.* 2022, 4, 1676−1683

Read Online

ACCESS | Metrics & More | Article Recommendations | Supporting Information

ABSTRACT: Since the chemical and thermal stability of organic thin film layers in organic light-emitting diodes (OLEDs) highly influences the operational device lifetime, a rational advanced design of materials and device structures is quite necessary. Here, we report a significant improvement in the device thermal stability and operational lifetime of blue-fluorescent OLEDs by adopting a mixed electron transporting layer (mETL) of 4,7-diphenyl-1,10-phenanthroline (BPhen) and hydroxyquinolinolato-lithium (Liq). Compared to pristine BPhen film, Liq mixing improved thermal and morphological stabilities of the mETL by increasing the glass-transition temperature and inhibiting crystallization of the ETL, which directly leads to better device performances. Compared to the reference device using the pristine BPhen film as an ETL, the device with mETL containing 50% Liq maintains the device characteristics, with respect to the thermal stress up to 110 °C, which is a 60 °C increase in the thermal stability of the blue device by applying mETL. Accordingly, the operational lifetime of the device with mETL containing 50% Liq is substantially extended by 67 times, ensuring that this remarkable device lifetime enhancement is dominantly driven by the improved thermal and morphological stabilities of mETL.

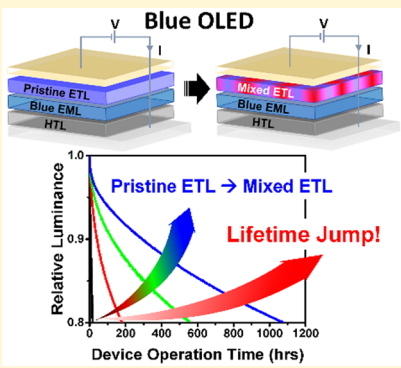

Since the last decades, the use of organic light-emitting diodes (OLEDs) in mobile display applications and televisions, as well as solid-state lighting, has become very common and successful in the market. One of the most critical factors to commercialize OLEDs is the stable operational device lifetime, which is mainly dependent on the chemical and physical stabilities of organic π-conjugated materials in the device.[1] In particular, thermal instability of materials in the OLED active layers may result in device degradation.[2] Generally, temperature increases during the operation can induce morphological changes to the organic materials in the OLED devices and may promote local crystallization in the OLED layers, which limits the lifespan of the devices.[3] Since the thermal stability of organic materials is closely correlated to the glass-transition temperature (T_g), a simple way to improve the morphological stability of organic thin film layers is by adapting existing materials having higher T_g or developing new organic materials with higher T_g.[4,5] Another efficient method is mixing an existing low T_g material with a higher T_g material, which can enhance the thermal and morphological stabilities of the thin film, with a T_g value between the two extremes.[6]

4,7-Diphenyl-1,10-phenanthroline (BPhen) has widely been used as an electron transporting layer (ETL), because of its high electron mobility and easy processability.[7] In addition, it is known that the electrical conductivity of BPhen can be enhanced by doping alkali metals or alkali-metal compounds.[8−10] The use of electron or hole transporting materials doped with another material is a very effective method for tuning the charge injection and transporting properties in organic semiconductor devices.[11−13] However, BPhen has a relatively low glass transition temperature (T_g = 62 °C) and crystallization occurs spontaneously in its film, reducing the

Received: July 2, 2022
Accepted: July 25, 2022
Published: August 1, 2022

Downloaded via 63.147.34.5 on April 2, 2025 at 08:55:50 (UTC).
See https://pubs.acs.org/sharingguidelines for options on how to legitimately share published articles.

ACS Publications © 2022 American Chemical Society

https://doi.org/10.1021/acsmaterialslett.2c00583
ACS Materials Lett. 2022, 4, 1676−1683

Pictiva EX2104
Samsung v Pictiva
IPR2026-00129

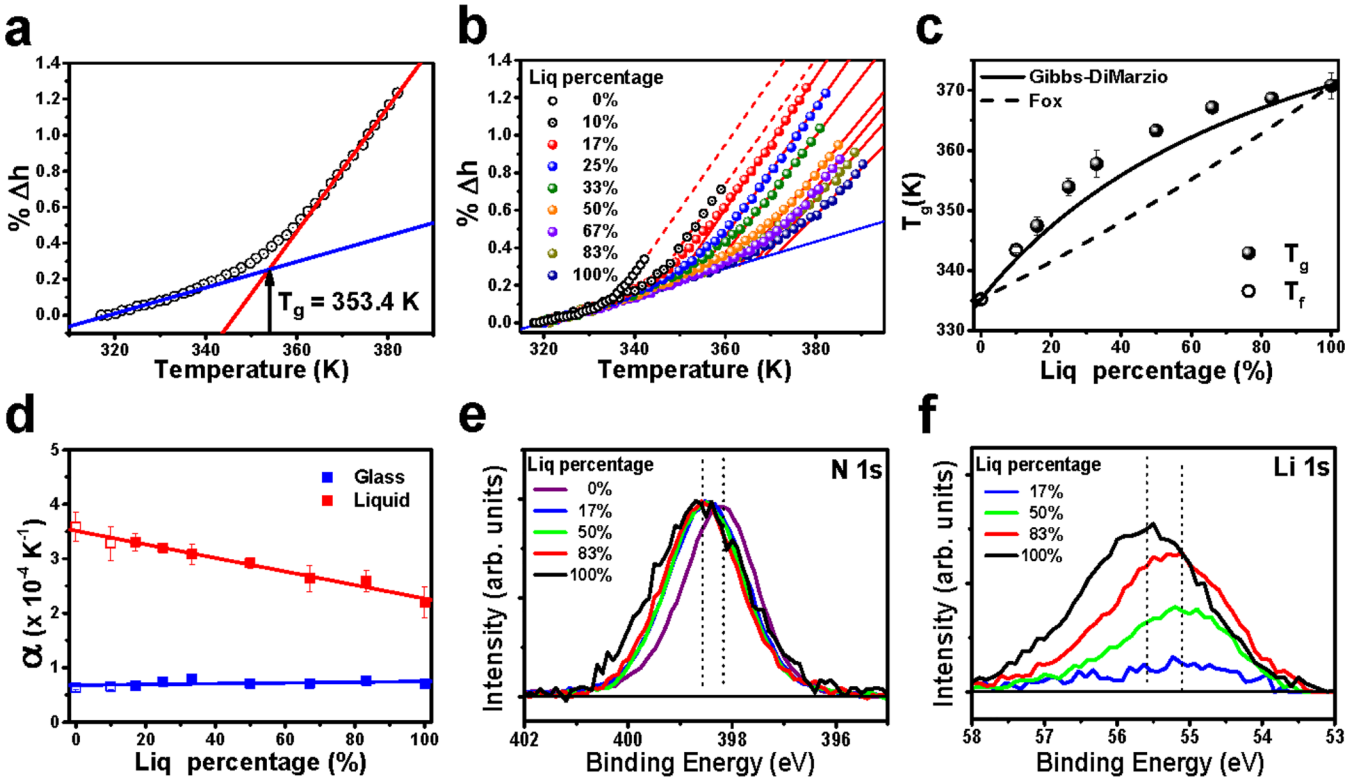

Figure 1. Temperature dependences of percentage thickness change (%Δh) for (a) 25% Liq mixed Liq:BPhen film and (b) Liq:BPhen films with different mixing percentage from 0 to 100% Liq. (c) Glass-transition temperatures (T_g) and (d) thermal expansion coefficients of glass and supercooled liquid states of films with varying compositions. X-ray photoelectron spectroscopy (XPS) spectra of (e) N 1s and (f) Li 1s for the mixture films of Liq and BPhen with various compositions are also shown.

device lifetime. A recent study reported that the thermal stability of OLEDs could be enhanced by doping cesium (Cs) to the BPhen film.[14] However, highly reactive metals, such as Li and Cs, have a tendency to diffuse readily through the organic thin film layers, thus harming the device lifetime.[3] Instead, a less-reactive lithium-metal-based organic molecule, 8-hydroxyquinolinolato-lithium (Liq), can be used to suppress this type of diffusion in the organic thin film layers.[15]

There had been some attempts to improve the device lifetime by mixing Liq with various ETL materials other than BPhen.[14−21] A previous OLED study based on the thermally activated delayed fluorescent (TADF) emitters[16] reported 16 times elongation of operation lifetime of the device, which was achieved by the combined effect of introducing an ultrathin Liq interlayer and a mixed host system in the device structure. Choi et al.[17] and Chiba et al.[18] also reported that the devices with Liq-doped ETL or EIL exhibited somewhat improved operational lifetime. However, those results are not sufficient to discuss the structure−property correlations of mixed organic layers and their device characteristics for small molecular OLEDs. In any case, the maximum operational lifetime enhancement only by applying Liq mixing with ETL or EIL did not exceed 6-fold.

Therefore, we investigated the mixing effect of BPhen and Liq on the glass transition temperature (T_g) and the crystallization behavior of their thin films. Furthermore, blue-fluorescent OLED devices were fabricated using the mixtures of BPhen and Liq (up to 50%) as a mixed electron transporting layer (mETL) to explore the improvement of device performance upon Liq mixing. The T_g value of the mETL increased as the percentage of Liq increased and mixing Liq with BPhen improved the morphological stability of mETL by inhibiting crystallization. The critical role of the thermal and morphological stabilities of mETL in the OLEDs, which are crucial to achieve the better device stability with a prolonged operational lifetime, was emphasized.

Unlike crystalline films where the melting transition determines the catastrophic failure of the organic layers, glass transition determines the integrity of the amorphous films as the glass transition is defined as the marked change between the supercooled liquid and the amorphous solid. The glass transition temperature (T_g) was measured through spectroscopic ellipsometry, which has the advantage of determining T_g from as-deposited films with a greater (>10^3 times) sensitivity, compared to conventional differential scanning calorimetry (DSC).[22−26] Each film of ∼200 nm was deposited on silicon wafer substrates by a thermal coevaporation at a deposition rate of ∼2 Å s^{-1} and the substrate temperature during the deposition process was not controlled meaning that the deposition temperature of the films ranged from 0.80T_g to 0.89T_g, depending on the mixing ratio. Although there are reports of films with ultrastable properties, such as higher density compared to those of ordinary glass, may form at the similar deposition temperatures relative to T_g,[27−29] no evidence of ultrastable behavior was observed in the current study, judging from the thickness change after the first temperature cycle. The sample was heated and cooled at rates of 10 °C min^{-1} and 5 °C min^{-1}, respectively. Typically, three temperature cycles were performed and T_g was determined from the cooling scans after the first run. (See Supporting Information for details.)

https://doi.org/10.1021/acsmaterialslett.2c00583
ACS Materials Lett. 2022, 4, 1676−1683
Pictiva EX2104
Samsung v Pictiva
IPR2026-00129

Figure 1a shows typical temperature dependent thickness data for the 25% Liq mixed film upon cooling obtained from spectroscopic ellipsometry. Red and blue lines in the figure represent the linear fits to the temperature dependent thicknesses of supercooled liquid and glass, respectively, and thermal expansion coefficients and T_g were determined through the fit lines. The temperature dependences of percentage thickness change (%Δh) for the mixed films with the varying mixing percentage from 0% to 100% are presented in Figure 1b. In Figure 1d, the thermal expansion coefficients of the glassy states were invariant with the composition, whereas those of supercooled liquid states linearly decreased as the Liq mixing percentage increased. (See Supporting Information for details.)

Figure 1c shows the T_g of pristine BPhen and Liq and their mixed films with varying mixing ratios. For the pristine BPhen and 10% Liq mixed films, the fictive temperatures (T_f), which were obtained from the first temperature ramping scans, were plotted instead of T_g as rapid and spontaneous crystallization occurred above T_g after the first heating scans. The fictive temperature (T_f), which is defined as the intersection temperature between the temperature dependence of glass thickness upon ramping and extrapolated that of equilibrium supercooled liquid thickness, usually has similar values compared to T_g for an ordinary glass. The value differences between T_g and T_f for the current system above 17% Liq mixing, where no crystallization was observed, were found to be within a degree. In addition, T_f measured in the study for the pristine BPhen (T_f = 335.2 ± 0.7 K) showed similar value to the T_g value measured by DSC ($T_{g,DSC}$ = 335.2 K).[6] For the pristine Liq, although it is well-known that the powder form of Liq is crystalline, as evidenced by the X-ray diffraction (XRD) pattern,[30,31] thermally evaporated films did not show any evidence of crystal formation by XRD, reflection polarization optical microscopy, and AFM measurements unless Liq was stored at ambient conditions for a certain amount of time.[32] Ellipsometry results of thermal deposited Liq film were consistent with the glass transition behavior of amorphous films (Figure 1b).

As shown in Figure 1c, as the percentage of Liq increased, T_g increased and approached T_g of pristine Liq. The curved lines plotted in the Figure 1c are based on predictions from Fox[33] and Gibbs and DiMarzio[34,35] on T_g for amorphous mixture films. The Fox equation predicts T_g based on the free volume change upon mixing, which is related to the size of the molecules, while the Gibbs−DiMarzio equation utilizes the change in conformational entropy in estimating T_g. Figure 1c shows that the trend of T_g variations upon mixing was closer to the prediction of Gibbs and DiMarzio than that of Fox, which implies that interaction adjustment due to the different species of molecules neighboring each other was more important in determining T_g than the free volume adjustment due to the size differences. This trend implies that the increase in the thermal stability of mixed film could be achieved with less mixing of Liq with BPhen.

The positive deviation of measured T_g from the Gibbs−DiMarzio prediction may indicate the increased interaction between BPhen and Liq molecules, and X-ray photoelectron spectroscopy (XPS) was performed to investigate molecular interaction between BPhen and Liq. Figures 1e and 1f show the XPS for N 1s and Li 1s peak of several mixture films. In case of BPhen, the N 1s peak of pristine BPhen sample was centered at 398.2 eV, which could be assigned to sp^2 hybridized pyridinic nitrogen in the BPhen molecule.[36,37] When BPhen was mixed with Liq (17%−83%), the binding energy of N 1s peak increased to 398.6 eV, having similar peak position with the 100% Liq film. In the case of 100% Liq, a small shoulder also appeared on the higher binding energy region, compared to the mixture films, which can be attributed to the formation of various coordination complexes when Liq exists alone resulting in a complicated electronic state of nitrogen.[31,38] Interestingly, the N 1s spectra of the mixture films cannot be fully deconvoluted with the N 1s spectra of pristine Liq and Bphen (see Figure S4 in the Supporting Information), implying that Liq and Bphen are not simply in their physical mixture, but their chemical interaction exists in the mixture.

In the Li 1s spectra, 100% Liq showed a peak at 55.6 eV. When 17% of Bphen was mixed to Liq, a red-shift of Li 1s peak to 55.1 eV was observed and no additional shifts were observed as the molar ratio of Bphen increased further. The synchronous peak shifts observed in N 1s and Li 1s spectra upon mixing Bphen and Liq, the binding energy increase in N 1s from pristine Bphen (∼0.4 eV) and the binding energy decrease in Li 1s from 100% Liq (∼0.5 eV), imply some chemical interaction between the N atoms (Bphen) and the Li atom (Liq). Binding energy of a core level electron from a molecule can increase when its valence electrons are withdrawn and vice versa.[39] As it has been reported that the interaction of Li atom with pyridinic N atom could increase the binding energy of N 1s,[40] in our case, it is possible that the lone-pair electrons of nitrogen in BPhen are partially transferred to the lithium of Liq in the mixture, forming stronger interaction between mixed components, which could increase the binding energy of N 1s and decrease the binding energy of Li 1s. A plausible explanation is that the lithium in Liq, which has a very high ion mobility, can interact efficiently with the pyridinic nitrogen of Bphen, even from a low concentration, 17% in our case, resulting in the overall similar chemical nature of nitrogen in the mixture films with that in the pristine Liq.

We note that this intermolecular interaction between the N atoms in BPhen and Li atom in Liq could be responsible for the positive deviation of T_g from the Gibbs−DiMarzio prediction as the glass transition of small-molecule glass former is related to the reorientation of the molecule. As the increased intermolecular interaction between mixed components is formed, the reorientation of this complex would be more restricted than the reorientation of each components.

Despite its superior electron mobility among known ETLs,[41] BPhen suffers from morphological instabilities that are due to a fast crystallization, which is facilitated by the relatively low T_g (62 °C) and its relative planar molecular structure.[42,43] The crystallization of the organic layer of OLED devices can lead to electrical shorts, which will eventually reduce the device yield and shorten the lifetime.[3,44] It is generally known that the doping could inhibit crystallization and have been utilized in stabilizing active layers in organic devices.[43,45,46] Thus, in addition to the increase in the T_g value of mixed films, mixing Liq with BPhen can limit the crystallization and improve the overall device performance. Since ambient conditions and high temperatures could promote crystallization, both encapsulated and as-deposited samples were produced and stored either at room temperature or ∼20 °C above the T_g value of each mixed film for as long as 5 days. Encapsulated samples showed a similar crystallization behavior as those stored under vacuum conditions.

https://doi.org/10.1021/acsmaterialslett.2c00583
ACS Materials Lett. 2022, 4, 1676−1683
Pictiva EX2104
Samsung v Pictiva
IPR2026-00129

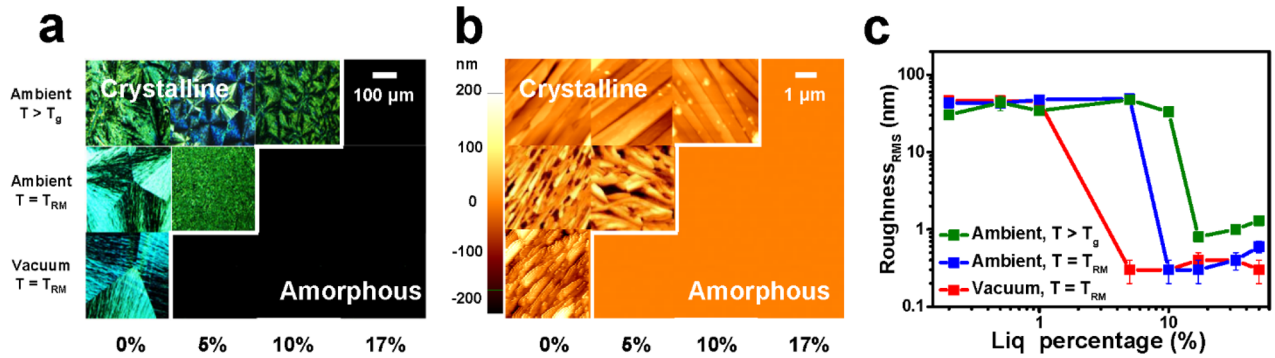

Figure 2. (a) Reflection polarization optical microscopy images, (b) AFM images, and (c) RMS roughness of mixed films of BPhen and Liq (up to 50%) with various compositions and under different storage conditions.

Scheme 1. Blue OLED Device Structure and Molecular Structure of BPhen, Liq, BH, BD, HAT-CN, HT1, and HT2

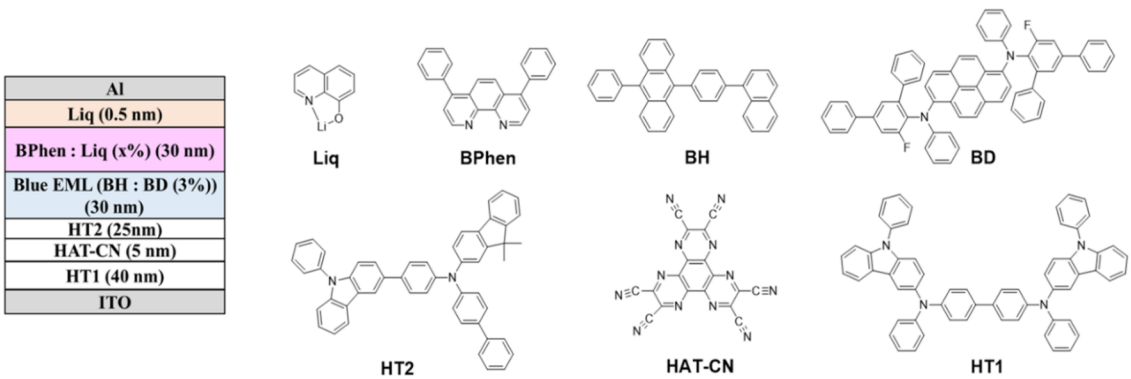

The morphological stabilities of mETLs upon different thermal treatments and storage conditions were investigated by examining the crystallization behavior using a custom-built reflection polarization optical microscopy system and atomic force microscopy (AFM). As seen in Figures 2a and 2b, an encapsulated sample of pristine BPhen that was stored at room temperature crystallized during the storage. Usually, the crystallization process can be observed within 2 h after deposition and the entire sample crystallizes within 6 h, which is similar to what has been reported previously.[42,47] Encapsulated BPhen film mixed with 5% Liq resisted crystallization at room temperature whereas the film with the same mixing percentage without the environmental protection crystallized within 2 days and 30 min at room temperature and temperatures above T_g, respectively. The BPhen film mixed with 10% Liq crystallized only at elevated temperatures, and films with the mixing percentage ranging from 17% to 50% resisted the morphological change, regardless of the storage conditions. The root-mean-square (RMS) roughness of samples was further studied using AFM. The encapsulated samples were measured within 3 min after stripping off the environmental protection glass cover. Figure 2c indicates that the amorphous film possessed the RMS roughness corresponding to the molecular level flatness (0.5 ± 0.2 nm), which confirmed the morphological integrity of the film at the molecular level. AFM images that show the morphologies of amorphous films are provided in the Supporting Information (Figure S3). On the other hand, the films that appeared as crystallized in the reflection polarization optical microscope and AFM showed a RMS roughness of 42.4 ± 3.6 nm on average.[47−49] This trend of RMS roughness is invariant with Liq mixing percentage under the vacuum storage condition, but shows a slight increase with Liq mixing percentage under ambient conditions and high temperatures, possibly due the sensitivity of alkali metals to moisture which led to surface degradation.[50] In any case, film XRD measurements showed no evidence of crystallization in the films that appeared to be amorphous in the reflection polarization optical microscopy and AFM.

To investigate the effect of mETL of BPhen and Liq on the OLED device performance, blue-fluorescent OLED devices were fabricated using mETLs with different mixing ratios and were compared to devices consisting of pristine BPhen, as an ETL. All organic and metal layers were thermally deposited in succession in a high-vacuum (ca. 10^{-7} Torr) system without breaking the vacuum. Then, the fabricated devices were encapsulated with cavity glass lids in a nitrogen-purged glovebox. The blue-fluorescent device structure was ITO/N4,N4′-diphenyl-N4,N4′-bis(9-phenyl-9H-carbazol-3-yl)-[1,1′-biphenyl]-4,4′-diamine (HT1) (40 nm)/1,4,5,8,9,11-hexaazatriphenylene hexa-carbonitrile (HAT-CN) (5 nm)/N-([1,10-biphenyl]-4-yl)-9,9-dimethyl-N-(4-(9-phenyl-9H-carbazol-3-yl) phenyl)-9H-fluoren-2-amine (HT2) (25 nm)/blue EML (30 nm)/BPhen:Liq mixed layer (30 nm)/Liq (0.5 nm)/Al. For the blue EML, 9-(4-(naphthalen-1-yl)phenyl)-10-phenylanthracene (BH) used as a blue host and N1,N6-bis(5′-fluoro-[1,1′:3′,1′′-terphenyl]-4′-yl)-N1,N6-diphenylpyrene-1,6-diamine (BD) as a blue-fluorescent emitter, which was 3% doped in the blue host. (See Scheme 1 and the Supporting Information.)

Since it is widely known that OLED devices should demonstrate a suitable temperature stability at least in the range of 70−90 °C for commercial applications,[3,51] the full device performances upon thermal stress were investigated by

https://doi.org/10.1021/acsmaterialslett.2c00583
ACS Materials Lett. 2022, 4, 1676−1683
Pictiva EX2104
Samsung v Pictiva
IPR2026-00129

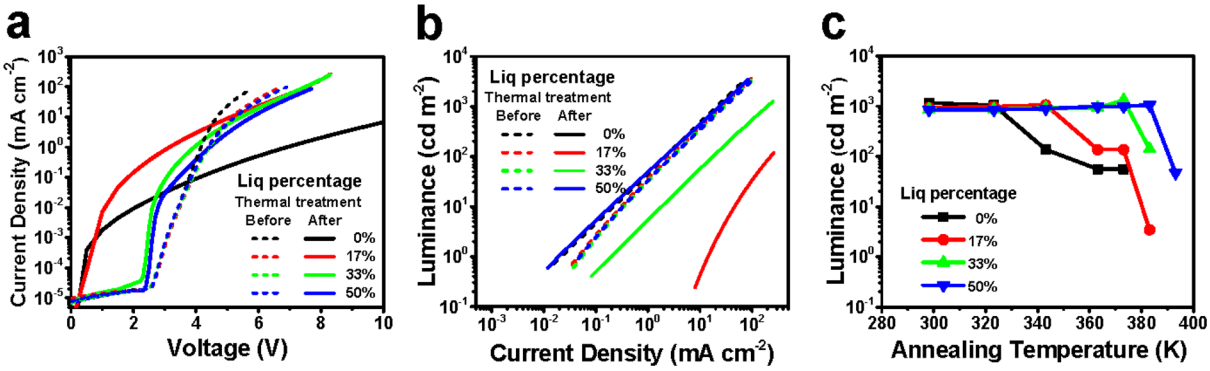

Figure 3. (a) Current density versus driving voltages and (b) luminances versus current density for blue devices using the mETL with different mixing ratio of BPhen and Liq, before (dashed lines) and after (solid lines) annealing at 110 °C for 60 min. (c) Variation in the luminance at 25 mA cm^{-2}, according to the annealing temperature applied to the blue devices.

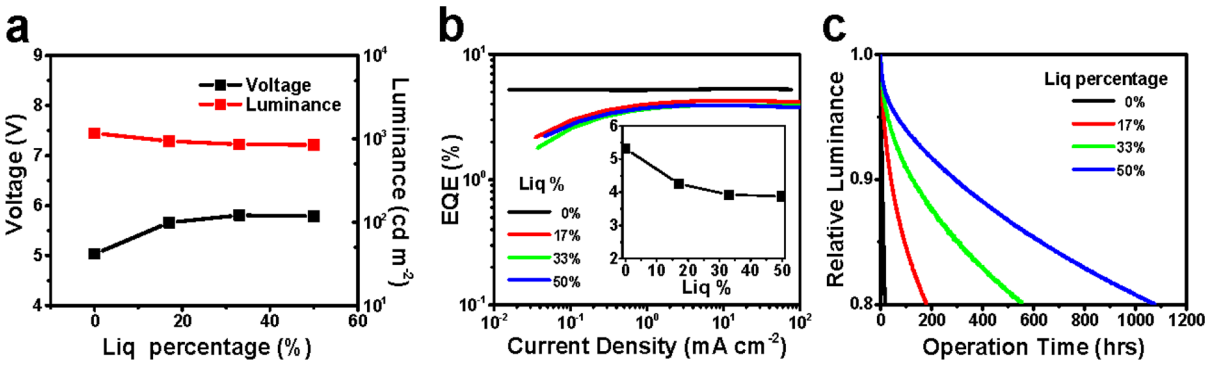

Figure 4. (a) Driving voltages, luminance, and (inset of panel (b)) external quantum efficiency (EQE) of the blue devices upon mixing percentage of Liq in the mETL under a constant current density of 25 mA cm^{-2}. (b) External quantum efficiency (EQE) versus current density for the devices upon mixing percentage of Liq in the mETL. (c) Relative luminance over the operation time under a constant current density of 25 mA cm^{-2} for the devices upon mixing percentage of Liq in the mETL.

annealing devices at different temperatures ranging from room temperature to 120 °C, prior to measurements to test the device stability upon thermal treatment. Figures 3a and 3b show the comparison of the current density versus driving voltage and luminance versus current density characteristics of the blue devices, under conditions before and after thermal annealing at 110 °C for 60 min. The mixing percentage of Liq in BPhen films varied from 0% to 50% as indicated. Prior to the thermal treatment, these characteristics (dashed curves) of the blue devices showed similar behavior upon mixing ratio change in the mETL. The current density versus driving voltage and luminance versus current density characteristics of the devices with mETLs were almost identical to each other and those of the device with the pristine BPhen showed slight deviations from the trends in the range of higher voltage and lower current density for Figures 3a and 3b, respectively. However, the difference between the device with mETLs and pristine BPhen ETL seemed to be very minor, compared to the difference by the thermal treatment.

After the thermal treatment (solid curves), the device with pristine BPhen ETL showed a sharp increase in the driving voltage near 0.25 V and reached >10 V at the current density of 25 mA cm^{-2} which was the relevant current density that produced the luminance of ∼1000 cd m^{-2} for the untreated device. Then, no luminance was detected in the entire range of the current densities studied, indicating a catastrophic failure of the device after thermal annealing at 110 °C for 60 min, probably due to the grain boundaries formed by crystallization in the pristine BPhen ETL, as shown by reflection polarization optical microscopy and AFM studies (Figure 2), which limited electron transport in the pristine BPhen layer. However, the treated device with the mETL containing 50% Liq showed no change of the current density versus driving voltage and luminance versus current density characteristics, compared to the untreated device. These characteristics of the devices with 17% and 33% Liq showed in-between behaviors of the devices with pristine BPhen and 50% Liq.

In order to systematically investigate the thermal stability of the device upon using mETLs, the devices using both pristine BPhen as ETL and mETLs of different mixing ratios were annealed at different temperatures ranging from room temperature to 120 °C for 60 min and measured the luminance at 25 mA cm^{-2}. Figure 3c shows the luminance change at 25 mA cm^{-2}, according to the annealing temperatures ranging for the devices with different mixing ratios of BPhen and Liq in the mETLs. For the device with pristine BPhen ETL, the device maintains its luminance up to 50 °C annealing before it degrades at the higher-temperature annealing. As the mixing percentage of Liq increased, the annealing temperature at which the device could withstand the luminance became higher. The device with the mETL containing 50% Liq maintained the device characteristics up to an annealing temperature of 110 °C, which can be interpreted as a 60 °C improvement in the thermal stability of the device and is a result of the combined contribution from the increase in T_g and crystallization inhibition upon using

https://doi.org/10.1021/acsmaterialslett.2c00583
ACS Materials Lett. 2022, 4, 1676−1683
Pictiva EX2104
Samsung v Pictiva
IPR2026-00129

mETLs. Tables showing the driving voltage, the luminance, and the external quantum efficiency at 25 mA cm^{-2} according to the annealing temperatures for the devices with the different mixing ratios of BPhen and Liq in the mETLs are provided in the Supporting Information (Tables S4, S5, and S6).

The driving voltage and luminance versus the Liq percentage characteristics at the current density of 25 mA cm^{-2} for the untreated devices are shown in Figure 4a. The driving voltages and luminance of the devices using mETL respectively showed an increase (+33%) and a decrease (−14%), compared to the device with pristine BPhen, but showed similar values among the devices using mETLs of different mixing ratios. This increase in the driving voltages of the mETL device is consistent with the XPS analysis (see Figures 1e and 1f) where the lone-pair electrons of N atoms in BPhen transfers to the Li atom of Liq, resulting in a decrease in the electron transport of BPhen.[52,53] As shown in Figure 4b, external quantum efficiencies (EQEs) of the devices with mETLs were also similar, except that of the device with pristine BPhen. The inset shows the EQEs at the current density of 25 mA cm^{-2} for the devices with different mixing ratios of mETL and ETL with pristine BPhen, where the device with pristine BPhen ETL showed a 32% higher EQE value, compared to devices using mETL. Fast electron injection into the blue-emitting layer from the ETL could lead to higher luminous efficiency of the devices, since the hole mobility of hole transporting materials was generally faster than the electron mobility of electron transporting materials.[34,35]

Figure 4c shows the relative luminance over the operation time under a constant current density of 25 mA cm^{-2} for the blue devices with the mETL containing different mixing ratios of BPhen and Liq. The device lifetime was measured up to LT80 parameter, defining the time where the luminance decreased to 80% of the initial luminance (L_0) corresponding to ∼1000 cd m^{-2} for the devices in the present work. The lifetime of the blue devices changed dramatically with the different mixing percentage of BPhen and Liq in the mETL. The lifetime for the device with the pristine BPhen ETL was very poor, with an LT80 parameter of 16 h; however, the device lifetime significantly increased with the mixing percentage of Liq in BPhen as an mETL. The LT80 of the device with the mETL containing 50% Liq increased by 67-fold over that of the device with the pristine BPhen ETL. This 67-fold enhancement of the device lifetime is unprecedented in both magnitude and cause. In the previous studies of improving the device lifetime upon mixing Liq to various ETL materials,[15−18] the maximum enhancement solely by using mETL was less than a factor of 6 and the power efficiency improvement upon Liq mixing was postulated as the main source of the improved device lifetime. In this present work, we would like to stress that the drastic device lifetime improvement was achieved and can be mainly attributed to the combined effect of enhanced thermal and morphological stabilities of ETL (BPhen) mixed with Liq.

In summary, the Liq mixing increased the T_g value of the mixed films of BPhen and Liq more than what was predicted by Gibbs and DiMarzio, presumably due to the stronger intermolecular interaction between the N atoms in BPhen and the Li atom in Liq. In addition, the Liq mixing in the BPhen thin film inhibited the crystallization of the thin film, only 10% Liq mixing was required to avoid crystallization, even at elevated temperatures in a protected environment. Furthermore, the improved thermal and morphological stabilities of mETL resulted in the better thermal stability and the prolonged operational lifetime of blue devices. While the reference device with the pristine BPhen ETL showed a luminance loss upon thermal annealing above 50 °C, the device with mETL containing 50% Liq maintained the luminance up to 110 °C, because of the T_g increase and crystallization inhibition of BPhen by Liq mixing. In addition, the operational lifetime of the device with the mETL containing 50% Liq was extended by a factor of 67, compared to the reference device with the pristine BPhen ETL.

■ ASSOCIATED CONTENT

Supporting Information

The Supporting Information is available free of charge at https://pubs.acs.org/doi/10.1021/acsmaterialslett.2c00583.

Experimental details including materials and sample preparation, the glass-transition temperature measurements, reflection polarization optical microscopy, atomic force microscopy (AFM), and X-ray photoelectron spectroscopy (XPS) measurements; device fabrication and measurements; encapsulation procedure (PDF)

■ AUTHOR INFORMATION

Corresponding Authors

Ohyun Kwon − *Samsung Advanced Institute of Technology, Samsung Electronics Co., Ltd., Suwon-Si, Gyeonggi-do 16678, Republic of Korea*; orcid.org/0000-0002-9940-0826; Email: o.kwon@samsung.com

Byoungki Choi − *Samsung Advanced Institute of Technology, Samsung Electronics Co., Ltd., Suwon-Si, Gyeonggi-do 16678, Republic of Korea*; Email: byoungki.choi@samsung.com

Keewook Paeng − *Department of Chemistry, Sungkyunkwan University, Suwon 16419, Republic of Korea*; orcid.org/0000-0001-5837-621X; Email: paeng@skku.edu

Authors

Min Seok Ki − *Department of Chemistry, Sungkyunkwan University, Suwon 16419, Republic of Korea*

Myungsun Sim − *Samsung Advanced Institute of Technology, Samsung Electronics Co., Ltd., Suwon-Si, Gyeonggi-do 16678, Republic of Korea*

Kyuhyun Im − *Samsung Advanced Institute of Technology, Samsung Electronics Co., Ltd., Suwon-Si, Gyeonggi-do 16678, Republic of Korea*

Byeong Jun Cha − *Department of Chemistry, Sungkyunkwan University, Suwon 16419, Republic of Korea*

Young Dok Kim − *Department of Chemistry, Sungkyunkwan University, Suwon 16419, Republic of Korea*; orcid.org/0000-0003-1138-5455

Tae Young Jin − *Department of Chemistry, Sungkyunkwan University, Suwon 16419, Republic of Korea*

Complete contact information is available at: https://pubs.acs.org/10.1021/acsmaterialslett.2c00583

Author Contributions

[∇]These authors contributed equally to this work.

Author Contributions

The manuscript was written through contributions of all authors. All authors have given approval to the final version of the manuscript.

Notes

The authors declare no competing financial interest.

https://doi.org/10.1021/acsmaterialslett.2c00583
ACS Materials Lett. 2022, 4, 1676−1683

Pictiva EX2104
Samsung v Pictiva
IPR2026-00129

■ ACKNOWLEDGMENTS

This research was supported by Basic Science Research Program through the National Research Foundation of Korea (NRF) funded by the Ministry of Education (No. NRF-2019R1A6A1A10073079).

■ REFERENCES

(1) Hong, G.; Gan, X. M.; Leonhardt, C.; Zhang, Z.; Seibert, J.; Busch, J. M.; Brase, S. A Brief History of OLEDs-Emitter Development and Industry Milestones. *Adv. Mater.* **2021**, *33*, 2005630.

(2) Kondakov, D. Y.; Sandifer, J. R.; Tang, C. W.; Young, R. H. Nonradiative recombination centers and electrical aging of organic light-emitting diodes: Direct connection between accumulation of trapped charge and luminance loss. *J. Appl. Phys.* **2003**, *93*, 1108−1119.

(3) Scholz, S.; Kondakov, D.; Lussem, B.; Leo, K. Degradation Mechanisms and Reactions in Organic Light-Emitting Devices. *Chem. Rev.* **2015**, *115*, 8449−8503.

(4) Steuber, F.; Staudigel, J.; Stossel, M.; Simmerer, J.; Winnacker, A.; Spreitzer, H.; Weissortel, F.; Salbeck, J. White light emission from organic LEDs utilizing spiro compounds with high-temperature stability. *Adv. Mater.* **2000**, *12*, 130−133.

(5) Tokito, S.; Tanaka, H.; Noda, K.; Okada, A.; Taga, Y. Thermal stability in oligomeric triphenylamine/tris(8-quinolinolato) aluminum electroluminescent devices. *Appl. Phys. Lett.* **1997**, *70*, 1929−1931.

(6) D'Andrade, B. W.; Forrest, S. R.; Chwang, A. B. Operational stability of electrophosphorescent devices containing p and n doped transport layers. *Appl. Phys. Lett.* **2003**, *83*, 3858−3860.

(7) Naka, S.; Okada, H.; Onnagawa, H.; Tsutsui, T. High electron mobility in bathophenanthroline. *Appl. Phys. Lett.* **2000**, *76*, 197−199.

(8) Reineke, S.; Lindner, F.; Schwartz, G.; Seidler, N.; Walzer, K.; Lüssem, B.; Leo, K. White organic light-emitting diodes with fluorescent tube efficiency. *Nature* **2009**, *459*, 234−238.

(9) Khan, M A; Xu, W.; Khizar-ul-Haq; Bai, Y.; Wei, F.; Jiang, X Y; Zhang, Z L; Zhu, W Q Highly power efficient organic light-emitting diodes based on p-doped and novel n-doped carrier transport layers. *J. Phys. D: Appl. Phys.* **2007**, *40*, 6535.

(10) Ma, J.; Xu, W.; Jiang, X.; Zhang, Z. Organic light-emitting diodes based on new n-doped electron transport layer. *Synth. Met.* **2008**, *158*, 810−814.

(11) Lussem, B.; Keum, C.-M.; Kasemann, D.; Naab, B.; Bao, Z.; Leo, K. Doped organic transistors. *Chem. Rev.* **2016**, *116*, 13714−13751.

(12) Gaul, C.; Hutsch, S.; Schwarze, M.; Schellhammer, K. S.; Bussolotti, F.; Kera, S.; Cuniberti, G.; Leo, K.; Ortmann, F. Insight into doping efficiency of organic semiconductors from the analysis of the density of states in n-doped C-60 and ZnPc. *Nat. Mater.* **2018**, *17*, 439−444.

(13) Walzer, K.; Maennig, B.; Pfeiffer, M.; Leo, K. Highly efficient organic devices based on electrically doped transport layers. *Chem. Rev.* **2007**, *107*, 1233−1271.

(14) Keum, C. M.; Kronenberg, N. M.; Murawski, C.; Yoshida, K.; Deng, Y.; Berz, C.; Li, W.; Wei, M.; Samuel, I. D.; Gather, M. C. The Role of Metallic Dopants in Improving the Thermal Stability of the Electron Transport Layer in Organic Light-Emitting Diodes. *Adv. Opt. Mater.* **2018**, *6*, 1800496.

(15) Kwon, J. H.; Lee, J. Y. High efficiency and long lifetime in organic light-emitting diodes using bilayer electron injection structure. *Synth. Met.* **2009**, *159*, 1292−1294.

(16) Tsang, D. P.-K.; Matsushima, T.; Adachi, C. Operational stability enhancement in organic light-emitting diodes with ultrathin Liq interlayers. *Sci. Rep.* **2016**, *6*, 22463.

(17) Choi, S. H.; Lee, S. J.; Lee, K. Y.; Yang, H. S.; Han, K.-i.; Kim, K. H.; Kim, S. D.; Bae, H. D.; Tak, Y. H. Improved efficiency and lifetime of organic light-emitting diode with lithium-quinolate-doped electron transport layer. *Jpn. J. Appl. Phys.* **2009**, *48*, 062101.

(18) Chiba, T.; Pu, Y. J.; Ide, T.; Ohisa, S.; Fukuda, H.; Hikichi, T.; Takashima, D.; Takahashi, T.; Kawata, S.; Kido, J. Addition of Lithium 8-Quinolate into Polyethylenimine Electron-Injection Layer in OLEDs: Not Only Reducing Driving Voltage but Also Improving Device Lifetime. *ACS Appl. Mater. Interfaces.* **2017**, *9*, 18113−18119.

(19) Xu, W.-D.; Lai, W.-Y.; Hu, Q.; Teng, X.-Y.; Zhang, X.-W.; Huang, W. A hydrophilic monodisperse conjugated starburst macromolecule with multidimensional topology as electron transport/injection layer for organic electronics. *Polym. Chem.* **2014**, *5*, 2942−2950.

(20) Wang, J.; Zhang, M.; Zhang, Y.; Fu, J.; Qin, Y.; Li, R.; Chen, Y.; Lai, W.; Zhang, X.; Huang, W. Efficient inverted organic light-emitting devices using a charge-generation unit as electron-injection layers. *Org. Electron.* **2021**, *96*, 106202.

(21) Chen, Y.; Chu, S.; Li, R.; Qin, Y.; Xu, Y.; Zhang, X.; Wang, J.; Liu, M.; Lai, W.-Y.; Huang, W. Highly efficient inverted organic light-emitting devices adopting solution-processed double electron-injection layers. *Org. Electron.* **2019**, *66*, 1−6.

(22) Dalal, S. S.; Sepulveda, A.; Pribil, G. K.; Fakhraai, Z.; Ediger, M. D. Density and birefringence of a highly stable alpha,alpha,beta-trisnaphthylbenzene glass. *J. Chem. Phys.* **2012**, *136*, 204501.

(23) Zhang, Y.; Fakhraai, Z. Invariant Fast Diffusion on the Surfaces of Ultrastable and Aged Molecular Glasses. *Phys. Rev. Lett.* **2017**, *118*, 066101.

(24) Yang, H. N.; He, S. J.; Zhang, T.; Man, J. X.; Jiang, N.; Wang, D. K.; Lu, Z. H. Glass transition temperatures in pure and composite organic thin-films. *Org. Electron.* **2018**, *60*, 45−50.

(25) Kearns, K. L.; Krzyskowski, P.; Devereaux, Z. Using deposition rate to increase the thermal and kinetic stability of vapor-deposited hole transport layer glasses via a simple sublimation apparatus. *J. Chem. Phys.* **2017**, *146*, 203328.

(26) Dalal, S. S.; Ediger, M. D. Molecular Orientation in Stable Glasses of Indomethacin. *J. Phys. Chem. Lett.* **2012**, *3*, 1229−1233.

(27) Ediger, M. D. Perspective: Highly stable vapor-deposited glasses. *J. Chem. Phys.* **2017**, *147*, 210901.

(28) Ediger, M. D.; de Pablo, J.; Yu, L. Anisotropic Vapor-Deposited Glasses: Hybrid Organic Solids. *Acc. Chem. Res.* **2019**, *52*, 407−414.

(29) Rodriguez-Tinoco, C.; Gonzalez-Silveira, M.; Ramos, M. A.; Rodriguez-Viejo, J. Ultrastable glasses: new perspectives for an old problem. *Riv. del Nuovo Cim.* **2022**, *45*, 325−406.

(30) Wang, X.; Shi, Z.; Li, B.; Li, D.; Zhuo, Y.; Wu, Z.; Li, S. 8-hydroxyquinoline lithium nanoribbons: synthesize and the photoconductivity sensing. *Optoelectron. Adv. Mater.—Rapid Commun.* **2011**, *5*, 1256−1259.

(31) Painuly, D.; Masram, D. T.; Rabanal, M. E.; Nagpure, I. M. The effect of ethanol on structural, morphological and optical properties of Li(I) 8-hydroxyquinoline phosphor. *J. Lumin.* **2017**, *192*, 1180−1190.

(32) Masumoto, Y.; Mori, T. Application of organic bathocuproine-based alloy film to organic light-emitting diodes. *Thin Solid Films* **2008**, *516*, 3350−3356.

(33) Fox, T. G., Jr.; Flory, P. J. Second-order transition temperatures and related properties of polystyrene. I. Influence of molecular weight. *J. Appl. Phys.* **1950**, *21*, 581−591.

(34) Dimarzio, E. A.; Gibbs, J. H. Molecular interpretation of glass temperature depression by plasticizers. *J. Polym. Sci., Part A: Gen. Pap.* **1963**, *1*, 1417−1428.

(35) Gibbs, J. H.; DiMarzio, E. A. Nature of the glass transition and the glassy state. *J. Chem. Phys.* **1958**, *28*, 373−383.

(36) Artyushkova, K. Misconceptions in interpretation of nitrogen chemistry from x-ray photoelectron spectra. *J. Vac. Sci. Technol.* **2020**, *38*, 031002.

(37) Kondo, T.; Guo, D. H.; Shikano, T.; Suzuki, T.; Sakurai, M.; Okada, S.; Nakamura, J. Observation of Landau levels on nitrogen-doped flat graphite surfaces without external magnetic fields. *Sci. Rep.* **2015**, *5*, 16412.

(38) Rajeswaran, M.; Begley, W. J.; Olson, L. P.; Huo, S. Steric effects of substituted quinolines on lithium coordination geometry. *Polyhedron* **2007**, *26*, 3653−3660.

https://doi.org/10.1021/acsmaterialslett.2c00583
ACS Materials Lett. 2022, 4, 1676−1682

Pictiva EX2104
Samsung v Pictiva
IPR2026-00129

(39) Egelhoff, W., Jr Core-level binding-energy shifts at surfaces and in solids. *Surf. Sci. Rep.* **1987**, *6*, 253−415.
(40) Bulusheva, L. G.; Kanygin, M. A.; Arkhipov, V. E.; Popov, K. M.; Fedoseeva, Y. V.; Smirnov, D. A.; Okotrub, A. V. In Situ X-ray Photoelectron Spectroscopy Study of Lithium Interaction with Graphene and Nitrogen-Doped Graphene Films Produced by Chemical Vapor Deposition. *J. Phys. Chem. C* **2017**, *121*, 5108−5114.
(41) Jou, J.-H.; Weng, J.-W.; Chavhan, S. D.; Yadav, R. A. K.; Liang, T.-W. Investigation of charge-transporting layers for high-efficiency organic light-emitting diode. *J. Phys. D: Appl. Phys.* **2018**, *51*, 454002.
(42) Han, S. L.; Wang, L. D.; Lei, G. T.; Qiu, Y. A study on the performances of white organic light-emitting diodes and the morphologies of their hole-blocking layers. *Jpn. J. Appl. Phys.* **2005**, *44*, L182−L185.
(43) D'Andrade, B. W.; Forrest, S. R.; Chwang, A. B. Operational stability of electrophosphorescent devices containing p and n doped transport layers. *Appl. Phys. Lett.* **2003**, *83*, 3858−3860.
(44) Ke, L.; Chua, S.-J.; Zhang, K.; Yakovlev, N. Degradation and failure of organic light-emitting devices. *Appl. Phys. Lett.* **2002**, *80*, 2195−2197.
(45) Peumans, P.; Bulovic, V.; Forrest, S. R. Efficient photon harvesting at high optical intensities in ultrathin organic double-heterostructure photovoltaic diodes. *Appl. Phys. Lett.* **2000**, *76*, 2650−2652.
(46) Peumans, P.; Bulovic, V.; Forrest, S. R. Efficient, high-bandwidth organic multilayer photodetectors. *Appl. Phys. Lett.* **2000**, *76*, 3855−3857.
(47) Chen, L.; Dong, G. F.; Duan, L.; Wang, L. D.; Qiao, J.; Zhang, D. Q.; Qiu, Y. One Order of Magnitude Enhancement of Electron Mobility by Rapid Cooling the Melt of an n-Type Organic Semiconductor. *J. Phys. Chem. C* **2009**, *113*, 16549−16552.
(48) Grover, R.; Srivastava, R.; Kamalasanan, M. N.; Mehta, D. S. Light outcoupling efficiency enhancement in organic light emitting diodes using an organic scattering layer. *Phys. Status Solidi Rapid Res. Lett.* **2014**, *8*, 81−85.
(49) Bin, Z.; Dong, G.; Wei, P.; Liu, Z.; Zhang, D.; Su, R.; Qiu, Y.; Duan, L. Making silver a stronger n-dopant than cesium via in situ coordination reaction for organic electronics. *Nat. Commun.* **2019**, *10*, 866.
(50) Xu, M. S.; Xu, J. B.; Luo, E. Z.; Xie, Z. Nanoscale investigation on nature of dark hole in moisture-exposed tris(8-hydroxyquinoline) aluminum thin films. *Chem. Phys. Lett.* **2003**, *374*, 656−660.
(51) Aziz, H.; Popovic, Z. D.; Hu, N. X. Organic light emitting devices with enhanced operational stability at elevated temperatures. *Appl. Phys. Lett.* **2002**, *81*, 370−372.
(52) Ding, L.; Sun, Y.-q.; Chen, H.; Zu, F.; Wang, Z.-K.; Liao, L.-S. A novel intermediate connector with improved charge generation and separation for large-area tandem white organic lighting devices. *J. Mater. Chem. C* **2014**, *2*, 10403−10408.
(53) Liu, C.; Zhang, D.; Duan, L. A novel anthracene derivative with an asymmetric structure as an electron transport material for stable Rec. 2020 blue organic light-emitting diodes. *J. Inf. Dispersion* **2020**, *21*, 197−201.

Recommended by ACS

Room-Temperature Continuous-Wave Microcavity Lasers from Solution-Processed Smooth Quasi-2D Perovskite Films with Low Thresholds

Xiang Gao, Lixiang Wang, *et al.*
MARCH 03, 2023
THE JOURNAL OF PHYSICAL CHEMISTRY LETTERS READ

Solid-State Lighting Using Side-by-Side White Phosphorescent Organic Light-Emitting Diodes

Claire Arneson, Stephen R. Forrest, *et al.*
JANUARY 27, 2023
ACS PHOTONICS READ

Versatile Use of 1,12-Diaminododecane as an Efficient Charge Balancer for High-Performance Quantum-Dot Light-Emitting Diodes

Seunghyun Rhee, Jeongkyun Roh, *et al.*
JANUARY 27, 2023
ACS PHOTONICS READ

Simplified Green-Emitting Single-Layer Phosphorescent Organic Light-Emitting Diodes with an External Quantum Efficiency > 22%

Fabien Lucas, Cyril Poriel, *et al.*
SEPTEMBER 14, 2022
CHEMISTRY OF MATERIALS READ

Get More Suggestions >

https://doi.org/10.1021/acsmaterialslett.2c00583
ACS Materials Lett. 2022, 4, 1676−1683

Pictiva EX2104
Samsung v Pictiva
IPR2026-00129